Half-cycle-like field-enhanced harmonic radiation by femtosecond laser-atom interaction

Cheng-Xin Yu, Shi-Bing Liu,* and Hai-Ying Song

Strong-Field and Ultrafast Photonics Lab, Institute of Laser Engineering, Beijing University of Technology, Beijing 100124, China

(Received 16 January 2013; published 10 June 2013)

A manipulatable half-cycle-like field (HCLF), homochromy with the driving femtosecond laser, is applied to enhance the harmonic emission by optimizing their relative delay time. We find that, by numerical computation, the HCLF can deliver a substantial momentum to the accelerated electrons as they return to their parent ions by a suitable phase delay, and also significantly increase the atomic ionization rate supplementarily. The results show that the harmonic order of the maximum or cut-off photon energy emitted in the presence of a half-cycle manipulating light pulse is risen to the 177th order, which is a significant increase compared with the 53rd order harmonics in the case of a single driving light pulse. To understand the essence from the wave-packet kinetics of the return electrons and their relation to the harmonic emission, we utilize the phase-space analysis of the coordinate momentum of an electronic wave packet by using a Gabor transformation, by which the presented numerical conclusions are further confirmed.

DOI: 10.1103/PhysRevA.87.063407 PACS number(s): 32.80.Rm, 42.65.Ky, 42.50.Hz

I. INTRODUCTION

High-order harmonic generation (HHG) has attracted growing interest of both experimentalists and theoreticians due to its unique plateau structure of spectrum, which can be utilized to generate soft x-ray sources and single attosecond pulses for real-time observation and steering of electronic dynamics on the atomic scale [1–5]. The process of HHG can be understood well by a semiclassical three-step model [6] and a quantum model [7]. Currently, two parallel hot topics concerning this field are improving the conversion efficiency from the driving light energy to the harmonics and increasing the cut-off photon energy emitted from the electron-ion recombination process, for which the phase matching between the driving and harmonic fields is considered a challenging condition [8,9]. Although extending the cut-off frequency can be made by using a longer-wavelength laser according to the cut-off rule [6], there is a significantly reduced harmonic yield [10,11]. Moreover, raising the laser intensity increases cut-off frequency at the cost of very high field ionization, and the resultant plasmas are responsible for the lower conversion efficiency. Hence seeking new approaches for the same expectations becomes a new interest of researchers.

In the classical models, the maximal energy or cut-off photon energy emitted is determined by the recollision energy of the accelerated electron in the laser field, which is given by (atomic units are used throughout) [12]

$$\Omega_{\max} = I_p + \kappa U_p,$$

where I_p and $U_p = E_L^2/(4\omega_o^2)$ are the atomic ionization potential and the electron quiver energy (ponderomotive energy), respectively, and $\kappa \approx 3.17$ for a monochromatic field E_L with an angular frequency ω_o [6,7]. The dynamics of the electrons accelerated by the laser field governs the cut-off frequency of harmonic emission. The assistant manipulation to the quantum paths of the returning electrons may be an achievable way to gain a larger return kinetic energy, in which the contribution of a manipulatable assistant pulse is to accelerate the ionized electrons and to drive them back to the nuclear core. Therefore, manipulation of the dynamics of electrons by adjusting the laser parameters, such as the carrier-envelope phase, chirp or pulse duration, etc., [13,14] come into use universally. It is clear that the emission spectrum is sensitive to the spectral composition of the applied driving light fields. To increase the value of κ, early in the 1990s, the methods of two-pulse and two-frequency HHG spectrum control were employed [12,15], while the idea of polarization control was first introduced by Corkum *et al.* [16].

Recently, approaches introducing a synthesized laser field composed of two or multicolors to improve the maximum emission energy by manipulating the relative time delay, phase differences, and ratios of strength between the multicolor fields have been applied frequently [17–24]. In addition, an optimal pulse with orthogonal two-color fields was also applied to select the electronic trajectory by manipulating their relative phase or other laser parameters [17,25–27].

Since it was generated experimentally [28], a terahertz half-cycle pulse (HCP) had been used widely in many aspects due to its asymmetric field [29–35]. It is worth noting that an HCP profile is a unipolar electric burst followed by a long and weak tail which ensures the zero time- integral of its electric field. Due to its sufficiently weak strength compared to the driving laser, the effects of the pulse tail on the atomic ionization processes and the dynamics of ionized electrons can be neglected. The biggest advantage of HCP is that it can deliver a nonzero momentum to a charged target during its lasting time regardless of how long its pulse duration is. The realization of a terahertz HCP provides an opportunity for generating HCPs with other frequency regimes, especially the midinfrared HCP.

Motivated by its unipolarity of HCP, we introduce a midinfrared HCLF into the strong-field-atoms interaction processes in this paper to increase the cut-off photon energy. It acts like an impulsive kick and can deliver a substantial momentum transfer to the accelerated electrons within an optical cycle, and its long and weak tail has been dropped out in our numerical calculations. The results demonstrate that the cut-off photon energy is significantly risen by optimizing

*Corresponding author: sbliu@bjut.edu.cn

the relative delay time between the driving and manipulating light pulses.

II. THEORETICAL MODEL

Without loss of generality, we solve numerically the one-dimensional time-dependent Schrödinger equation (TDSE) to investigate the HHG spectrum:

$$i\partial_t \Psi(x,t) = \left[-\partial_x^2/2 + V(x) + x\mathcal{E}(t)\right]\Psi(x,t),$$

where $x\mathcal{E}(t)$ describes the interaction between the intense laser field and the hydrogen atom under the dipole approximation in length gauge. Here, the soft Coulomb potential $V(x) = -q/\sqrt{x^2+A}$ with $q = 0.561$ and $A = 0.367$ yields ground-state energy $\epsilon_0 = -0.5$ a.u. and first excited-state energy $\epsilon_1 = -0.125$ a.u. for the hydrogen atom [36]. In our calculations, the spatial integration grid is confined in a finite space $-500 \leqslant x \leqslant 500$ a.u. with the number of grids 4096, which indicates the grid spacing of $\Delta x \approx 0.25$ a.u. The total length of the pulse is $T = 20$ fs, and the number of time steps is 8192 with the time step $\Delta t \approx 0.1$ a.u. In order to obtain the eigenstates of the zero-field Hamiltonian, we apply the Fourier grid Hamiltonian method based on the split-operator technique [37], and achieve $N_{\text{bound}} = 29$ bound states.

The synthesized field can be expressed as

$$\mathcal{E}(t) = E_d f_d(t)\cos(\omega_o t) + E_c f_c(t - t_{\text{delay}})\cos[\omega_o(t - t_{\text{delay}})],$$

where $E_d = 0.1$ a.u. and $E_c = \alpha E_d$ are the peak values of the driving and the manipulating electric field strength, respectively, and α is an adjustable parameter. The angular frequency $\omega_o = 0.0569$ a.u. corresponds to the wavelength 800 nm for the two pulses, and the relative time delay, t_{delay}, is defined as the difference between their pulse peaks, which is an adjustable optimized parameter. The Gaussian envelope of the two pulses are expressed as $f_d(t) = \exp(-t^2/t_{\text{df}}^2)$ and $f_c(t - t_{\text{delay}}) = \exp[-(t - t_{\text{delay}})^2/t_{\text{cf}}^2]$, respectively, where $T_L = 2\pi/\omega_o$ is the optical period of the laser pulse, t_{df} and t_{cf} are the temporal full width at half maximum of the driving pulse and manipulating pulse, respectively. In this paper, we choose $t_{\text{df}} = 5$ fs, and $t_{\text{cf}} = 0.4T_L$ to ensure that the manipulating pulse acts as an HCP, i.e., an HCLF. Its nonzero dc component can be compensated by adding a long and weak tail of practically opposite polarity [38], which does not change the dynamics of the concerned electrons significantly.

We assume that at $t = -10$ fs the atom is in its ground state, and the electronic wave function is propagated using the split-operator method [39] combined with fast Fourier transformation. To prevent spurious reflections from the spatial grid boundaries, at each time step, the total wave function is multiplied by a $\cos^{1/8}$-type mask function, which varies from 1 to 0 starting from the 3/4 of the grids.

Once the time-dependent wave function $\Psi(x,t)$ is obtained, one can calculate the time-dependent induced dipole acceleration as follows:

$$a(t) = \langle\Psi(x,t)|[-\partial V(x)/\partial x]|\Psi(x,t)\rangle - \mathcal{E}(t) \quad (1)$$

and the HHG power spectra as follows:

$$P(\omega) = \left|\frac{1}{T}\frac{1}{\omega^2}\int_{-T/2}^{T/2} a(t)e^{-i\omega t}dt\right|^2, \quad (2)$$

where T is the total length of the pulse.

III. RESULTS AND DISCUSSIONS

In Fig. 1(a), we depict the HHG spectrum in logarithmic scale by varying the time delay between the driving laser pulse that excites the bound electron to the continuum states, and an HCLF that is responsible for manipulating the trajectories of the ionized electrons. The value of κ is determined by $\kappa = (\Omega_{\text{max}} - I_p)/U_p$. It can be seen that there are three main peaks contributing to three extensions of cut-off frequencies of HHG, which are related to three optimized time delays, respectively. When the relative $t_{\text{delay}} = 0.075$ fs, the value of κ for the maximal return kinetic energy (RKE) is 12.48 corresponding to the harmonic order $N_{\text{max}} = 177$, while $\kappa = 3.17$ for the single driving pulse corresponds to the harmonic order $N_{\text{max}} = 53$. In addition, there are two other optimized

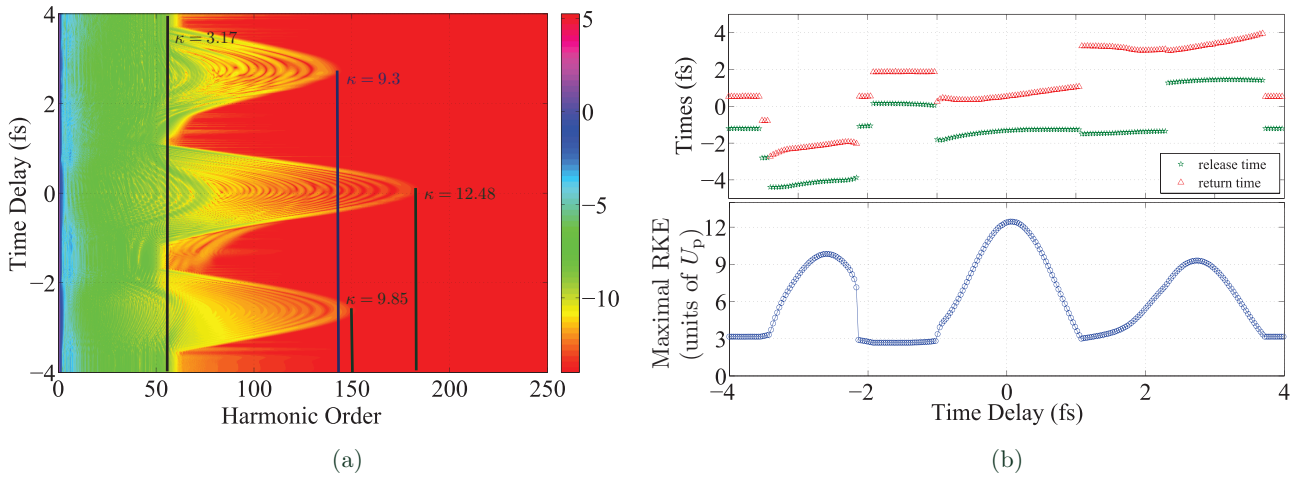

(a) (b)

FIG. 1. (Color online) (a) The spectra of HHG varying with the time delay by solving the TDSE. (b) The maximal return kinetic energies of ionized electrons and the corresponding release and return times, which are obtained from the classical calculation. Here the field ratio $\alpha = E_c/E_L = 1$.

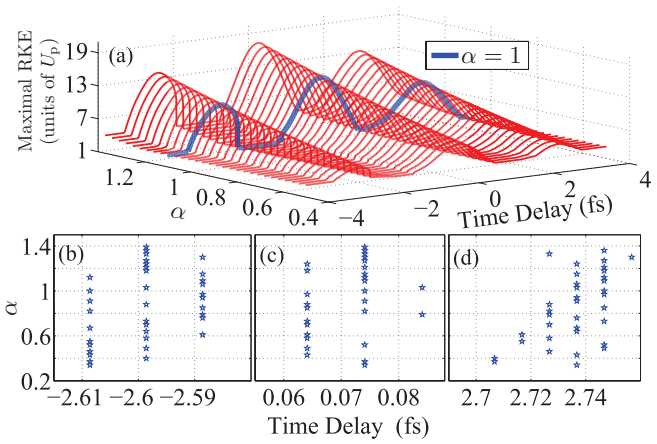

FIG. 2. (Color online) The maximal RKE for the optimal time delay and different amplitudes of manipulating pulse. (a) The maximal RKE for different values of α and the corresponding optimal time delay, where the blue line means $\alpha = 1$. The optimal time delay versus the field ratio α at (b) the first RKE, (c) the second RKE, and (d) the third RKE corresponding to Fig. 1(a).

values of time delay: $t_{\text{delay}} = -2.61$ fs, which gives $\kappa = 9.84$, and $t_{\text{delay}} = 2.70$ fs, which gives $\kappa = 9.3$. In this model, an electron is released from an atom through tunnel ionization and then driven by a nonsinusoidal combined laser field that breaks the dynamic symmetry of the electronic wave packet (EWP). As can be seen, the peaks of the manipulating pulse should lag shortly behind that of the driving pulse, and the main role of the manipulating pulse is to optimize the quantum path of the EWP.

For the sake of better understanding the role that the manipulating pulse plays, we also perform numerical calculations of the classical motion equations for an electron in the field. Under the strong-field approximation, the classical dynamics of an ionized electron is governed by Newton equation $\ddot{x}(t,t_i) = -\mathcal{E}(t)$, where t_i is the release time of the electron, and the double dots over x represent the second derivative with respect to the time t. Since an electron is assumed to be released in the laser field at t_i with zero velocity, by integration over $[t_i,t]$, one can easily obtain its velocity $v(t,t_i) = -\int_{t_i}^{t} \mathcal{E}(t')dt' = \mathcal{A}(t_i) - \mathcal{A}(t)$ and its displacement $x(t,t_i) = (t - t_i)\mathcal{A}(t_i) - \int_{t_i}^{t} \mathcal{A}(t')dt'$. Here, we have introduced the vector potential $\mathcal{A}(t)$ associated to $\mathcal{E}(t) = -d\mathcal{A}/dt$. The RKE of an ionized electron can be expressed as $E_{\text{kin}} = \frac{1}{2}[\mathcal{A}(t_1) - \mathcal{A}(t_i)]^2$, where the return time t_1 is determined by $x(t,t_i) = 0$, i.e., $\int_{t_i}^{t} \mathcal{A}(t')dt' = (t - t_i)\mathcal{A}(t_i)$. The maximal RKE can be obtained by $dE_{\text{kin}}/dt_i = 0$ [40], which gives $\mathcal{A}(t_i) = \mathcal{A}(t_1) - (t_i - t_1)\mathcal{E}(t_i)$, as shown in Fig. 1(b). In the upper panel of Fig. 1(b), we present the release (green pentagons) and return (red triangles) times of the electron that contribute to the maximal RKE. The corresponding RKE curve is also given in the lower panel. Classical calculations also confirm that it is possible to optimize the synthesizing pulse by adjusting the relative time delay between the two pulses. Since the field ratio between electric amplitudes of the two pulses is adopted as an adjustable parameter, we also calculate the maximal RKE for different values of $\alpha = E_c/E_d$ and obtain the corresponding optimal time delay, as shown

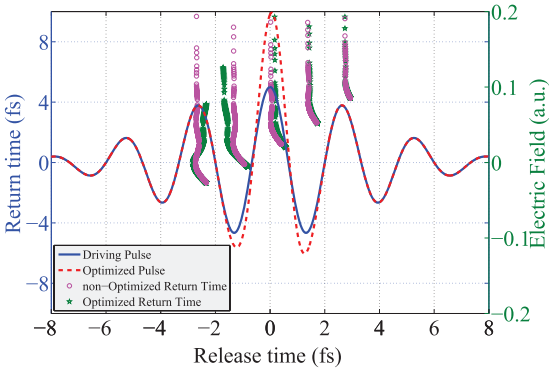

FIG. 3. (Color online) The classical electronic trajectory (black solid line) driven by the optimized synthesizing pulse with $t_{\text{delay}} = 0.075$ fs. As a comparison, the nonoptimized trajectory is also presented (the black dashed line).

in Fig. 2(a), and the blue line means $\alpha = 1$. Furthermore, Figs. 2(b)–2(d) present the relations between the optimal time delay and the field ratio α for the three different maximal RKEs. We can conclude from Fig. 2 that the pulse peak of the optimized HCLF always lies behind that of the driving laser pulse regardless of the amplitude of the HCLF. As an example, we only analyze the case $\alpha = 1$ without loss of generality in this paper.

From the classical point of view, the negative peak of driving pulse releases the electronic wave packet (if the laser field is strong enough), and then drives it away from the parent ion. After the driving pulse changes its direction, the ionized electron is decelerated. Meantime, the manipulating pulse is also transferring a substantial momentum and driving the electron to a further distance before it reaches the absorbing zones, which means the longest accelerative distance. Then the ionized electron is accelerated toward the nuclear core by the combined laser pulse, and the introduction of the manipulating pulse speeds the electron to the ion in a shorter time, as shown in Fig. 3.

In order to fully investigate the influence of the manipulating pulse on the electrons born at other times, we compare the release and return times of ionized electrons with (green pentagons) and without (magenta circles) the

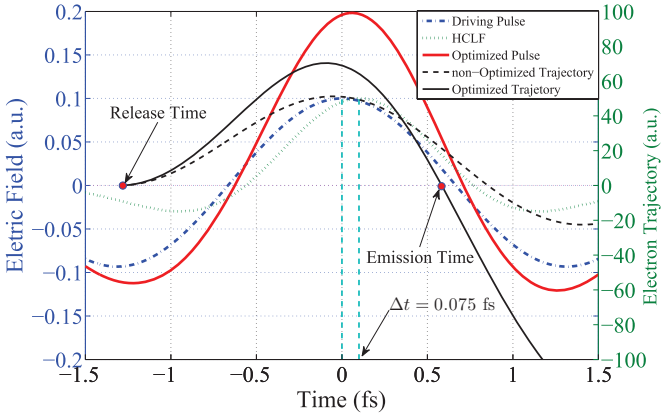

FIG. 4. (Color online) A comparison of return time between the ionized electrons by the laser field with and without manipulating pulse combined.

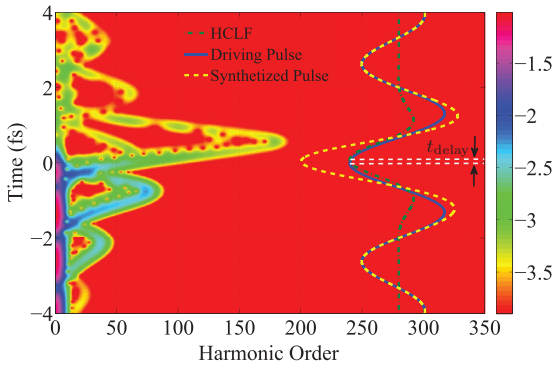

FIG. 5. (Color online) The time-frequency profile of the HHG power spectra of a hydrogen atom driven by the optimized synthesizing pulse with $t_{delay} = 0.075$ fs.

manipulating pulse included, which is shown in Fig. 4. For those electrons which are released between -2.6 and -2.2 fs and have undergone more than a cycle, the introduction of the manipulating pulse promotes their motion toward the nuclear core, and offers them another chance to recombine with the ions in a short time. The same is true for those induced by the driving laser between -1.8 and -1.2 fs, and the electron that contributes to the maximal RKE of $12.48U_p$ is also released in this time interval. In addition, the electrons produced between 0 and 0.17 fs are driven away from the ions by the combined laser field, and lose their opportunities of recombining with the ions. While the electrons released within 0.41–0.58 fs gain the chance to recombine with the ions during the last two optical cycles. Considering the fact that the atomic ionization rate monotonically increases with the increasing electric field, and the EWPs in continuum states spread very quickly, only those electrons ionized near the main peaks of the driving pulse can be selected as candidates for generating the harmonics of the extended cut-off frequencies.

To figure out the detailed spectral and temporal structures of HHG, we perform a time-frequency analysis by means of the Gabor transform of the induced dipole acceleration $a(t)$ [23],

$$a_G(\omega,t) = \int_{-\infty}^{\infty} \exp(i\omega t') \exp\left[-\frac{(t-t')^2}{2\sigma_0^2}\right] a(t')dt',$$

where σ_0 is the width of the Gaussian time window in the Gabor transformation, and we choose $\sigma_0 = 0.1$ fs in our calculation. Figure 5 shows a representative graph of the modulus of the time-frequency profile of the HHG spectra in logarithmic scale for hydrogen atoms driven by the optimized synthesizing pulse. In the extended plateau region, starting from the 100th-order harmonic, we note that the short-trajectory electrons make the major contributions to the extended plateau, which occurs from 0 to 1.2 fs. Moreover, from Fig. 5, the introduction of HCLF also enhances atomic ionization, and even causes ionization saturation after $t = 1$ fs. More importantly, since the HCLF selectively accelerates the ionized electrons, its utilization indicates a single HHG burst of extended frequencies, which is favorable for the synthesization of an isolated attosecond pulse.

Since the wave function $\Psi(x,t)$ contains all the information about the electronic dynamics, especially the position and velocity distribution, we can investigate the evolution of the electronic wave packet and make some predictions. To obtain a deeper insight into the HHG process, we propose a scheme by using the Gabor transformation,

$$\mathcal{Q}(x,p,t) = \int_{-\infty}^{+\infty} \Psi(x',t) \exp\left[-\frac{(x-x')^2}{2\delta_0^2}\right] e^{-ipx'} dx', \qquad (3)$$

where δ_0 is the width of the Gaussian coordinate window in the Gabor transform, and we choose $\delta_0 = 1.3$ a.u. in our numerical analysis. The modulus of $\mathcal{Q}(x,p,t)$ describes the instantaneous position and momentum of the electronic packets at t, as shown in the left panel of Fig. 6, while the right panel presents the corresponding profile of the electric fields. According to the position-momentum profile (PMP) analysis, particularly, it can be seen that the harmonics bursts of near-cut-off frequency last about $\tau \approx 222$ as. Therefore, the x-p phase-space analysis

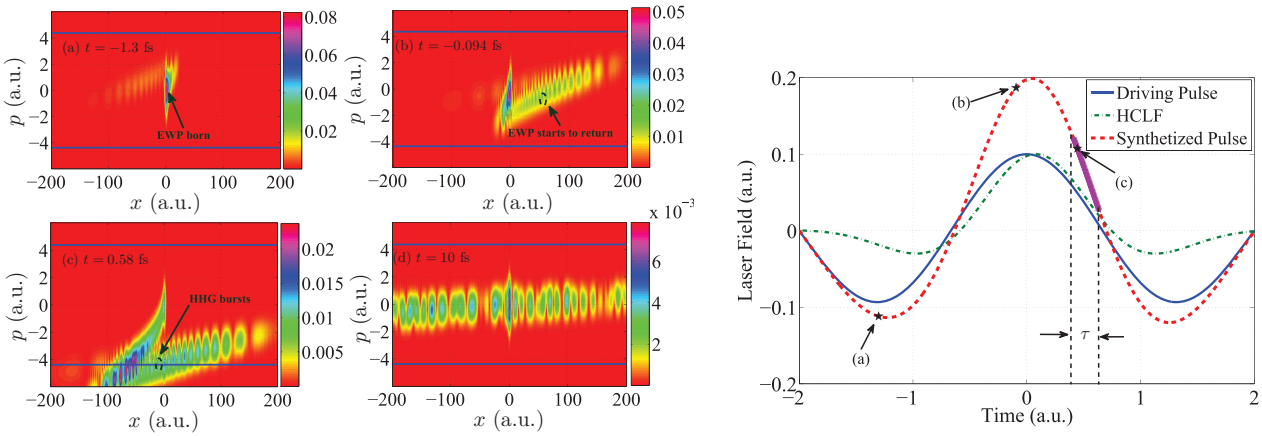

FIG. 6. (Color online) The left panel represents the PMP of the electronic wave packets at different moments: (a) $t = -1.3$ fs, the EWP that contributes to the harmonics of cut-off frequency is created; (b) $t = -0.094$ fs, the EWP reaches the furthest distance, and begins moving toward the ion under the combined pulses; (c) $t = 0.45$ fs, the harmonics bursts of the near-cut-off frequency are emitting, and the velocity (or momentum) can be evaluated as $p \approx \pm\sqrt{2\kappa U_p} = \pm 4.38$ a.u.; (d) the PMP of EWP at the end of the laser pulse, and the blue lines represent the maximal return velocity of electrons corresponding to the maximal RKE of $12.48U_p$. The right panel presents the corresponding electric fields, and the time interval that the HHG of near-cut-off frequency lasts is also roughly displayed, $\tau \approx 222$ as.

provides the spatial distribution and information about the flow of the electronic wave packet during the laser interaction, and informs us about the return momentum of the ionized electron.

The PMP indicates that, if $px < 0$, the EWP moves toward the parent ion, and if $px > 0$, the EWP is driven away from the ion, where the direction of motion depends on the sign of the momentum p. Considering the signal strength of the HHG and the maximal radiation frequency, the manipulating pulse should be turned on only when sufficient electrons are produced. In the single atomic approximation, it means that sufficient strong EWP is created and driven sufficiently far away from the ion before it moves into the absorbing zones. At $t \approx -1.3$ fs that is obtained from the classical motion equation of the ionized electrons, the EWP that contributes to the maximal RKE is released by the driving pulse, and is accelerated away from the ion toward a positive direction until the driving pulse changes its direction, shown in Fig. 6(a). Under the combined pulses consisting of the driving and manipulating pulses, the EWP being in continuum states is experiencing the deceleration, a fraction of the EWP probably escapes from the absorbing boundaries, and never returns to the ionic core. When $t \approx -0.094$ fs, the concerned fragment of the EWP arrives at the furthest position relative to the ion, shown in Fig. 6(b). Then the combined pulses provide enough energies to drive it to the parent ion. From about $t = 0.41$–0.63 fs, the EWP collides with the ion, and is captured at a certain probability as shown in Fig. 6(c). Meantime, the harmonics of the near-cut-off frequency are emitted as a result of electron-ion recombination. In Fig. 6(d), we give the PMP at the end of the laser pulse.

IV. CONCLUSIONS

In conclusion, due to its unique feature of unipolarity, an HCLF is combined with a driving laser pulse to extend the cut-off frequency of harmonic emission. This is because the HCLF can transfer a substantial momentum to an ionized electron during the second step of the rescattering process for HHG [6]. By adjusting the relative time delay between the pulses, we obtain an optimized condition that the cut-off frequency of the harmonics can be extended to $I_p + 12.48U_p$ for the hydrogen atom and the driving laser field $E_0 = 0.1$ a.u. In our computations, the TDSE in the dipole approximation and length gauge is solved numerically by using a split-operator method. The results indicate that the main contribution of the manipulating pulse is driving the EWP toward the atomic core accompanyied by the driving pulse rather than releasing the EWP through tunneling ionization. The time-frequency analysis shows that the introduction of a HCLF is beneficial for the synthesization of an isolated attosecond due to harmonic emission only within a single time interval. Moreover, we have proposed a method of position-momentum analysis by analogizing Gabor transformation between the coordinates and momentum of the EWP to the time-frequency analysis, in which the multiplication $px < 0$ represents the EWP moving toward the parent ion, $px > 0$ means the EWP moving away from the ion, and the direction of motion depends on the sign of the momentum p.

ACKNOWLEDGMENT

We acknowledge the support from the National Natural Science Foundation of China (Grant No. 10974010).

[1] P. M. Paul, E. S. Toma, P. Breger, G. Mullot, F. Augé, Ph. Balcou, H. G. Muller, and P. Agostini, Science **292**, 1689 (2001).
[2] R. Kienberger, E. Goulielmakis, M. Uiberacker, A. Baltuska, V. Yakovlev, F. Bammer, A. Scrinzi, Th. Westerwalbesloh, U. Kleineberg, U. Heinzmann, M. Drescher, and F. Krausz, Nature (London) **427**, 817 (2004).
[3] M. Hentschel, R. Kienberger, Ch. Spielmann, G. A. Reider, N. Milosevic, T. Brabec, P. Corkum, U. Heinzmann, M. Drescher, and F. Krausz, Nature (London) **414**, 509 (2001).
[4] C. Winterfeldt, C. Spielmann, and G. Gerber, Rev. Mod. Phys. **80**, 117 (2008).
[5] A. Baltuška, Th. Udem, M. Uiberacker, M. Hentschel, E. Goulielmakis, Ch. Gohle, R. Holzwarth, V. S. Yakovlev, A. Scrinzi, T. W. Häsch, and F. Krausz, Nature (London) **421**, 611 (2003).
[6] P. B. Corkum, Phys. Rev. Lett. **71**, 1994 (1993).
[7] M. Lewenstein, Ph. Balcou, M. Yu. Ivanov, A. L'Huillier, and P. B. Corkum, Phys. Rev. A **49**, 2117 (1994).
[8] T. Popmintchev, M. C. Chen, A. Bahabad, M. Gerrity, P. Sidorenko, O. Cohen, I. P. Christov, M. M. Murnane, and H. C. Kapteyn, Proc. Natl. Acad. Sci. USA **106**, 10516 (2009).
[9] A. Bahabad, M. M. Murnane, and H. C. Kapteyn, Nat. Photonics **4**, 570 (2010).
[10] W. Becker, S. Long, and J. K. McIver, Phys. Rev. A **50**, 1540 (1994).
[11] J. Tate, T. Auguste, H. G. Muller, P. Salières, P. Agostini, and L. F. DiMauro, Phys. Rev. Lett. **98**, 013901 (2007).
[12] S. Watanabe, K. Kondo, Y. Nabekawa, A. Sagisaka, and Y. Kobayashi, Phys. Rev. Lett. **73**, 2692 (1994).
[13] P. Zou, Z. N. Zeng, Y. H. Zheng, Y. Y. Lu, P. Liu, R. X. Li, and Z. Z. Xu, Phys. Rev. A **81**, 033428 (2010).
[14] P. C. Li, X. X. Zhou, G. L. Wang, and Z. X. Zhao, Phys. Rev. A **80**, 053825 (2009).
[15] Y. Y. Yin, C. Chen, D. S. Elliott, and A. V. Smith, Phys. Rev. Lett. **69**, 2353 (1992).
[16] P. B. Corkum, N. H. Burnett, and M. Y. Ivanov, Opt. Lett. **19**, 1870 (1994).
[17] L. Brugnera, D. J. Hoffmann, T. Siegel, F. Frank, A. Zaïr, J. W. G. Tisch, and J. P. Marangos, Phys. Rev. Lett. **107**, 153902 (2011).
[18] J. A. Párez-Hernández, D. J. Hoffmann, A. Zaïr, L. E. Chipperfield, L. Plaja, C. Ruiz, J. P. Marangos, and L. Roso, J. Phys. B **42**, 134004 (2009).
[19] R. F. Lu, H. X. He, Y. H. Guo, and K. L. Han, J. Phys. B **42**, 225601 (2009).
[20] S. S. Tang and X. F. Chen, Phys. Rev. A **85**, 063816 (2012).
[21] C. L. Xia, X. L. Ge, X. Zhao, J. Guo, and X. S. Liu, Phys. Rev. A **85**, 025802 (2012).
[22] Y. Xiang, Y. P. Niu, and S. Q. Gong, Phys. Rev. A **85**, 023808 (2012).

[23] K. J. Yuan and A. D. Bandrauk, J. Phys. B **45**, 074001 (2012).
[24] A. D. Bandrauk, S. Chelkowski, H. Yu, and E. Constant, Phys. Rev. A **56**, R2537 (1997).
[25] R. Murray, C. Ruiz, J. P. Marangos, and M. Yu Ivanov, J. Phys. B **43**, 135601 (2010).
[26] C. Ruiz, D. J. Hoffmann, R. Torres, L. E. Chipperfield, and J. P. Marangos, New J. Phys. **11**, 113045 (2009).
[27] L. Brugnera, F. Frank, D. J. Hoffmann, R. Torres, T. Siegel, J. G. Underwood, E. Springate, C. Froud, E. I. C. Turcu, J. W. G. Tisch, and J. P. Marangos, Opt. Lett. **35**, 3994 (2010).
[28] D. You, R. R. Jones, P. H. Bucksbaum, and D. R. Dykaar, Opt. Lett. **18**, 290 (1993).
[29] M. Machholm and N. E. Henriksen, Phys. Rev. Lett. **87**, 193001 (2001).
[30] A. Matos-Abiague and J. Berakdar, Phys. Rev. A **68**, 063411 (2003).
[31] E. Gershnabel, I. Sh. Averbukh, and R. J. Gordon, Phys. Rev. A **73**, 061401(R) (2006).
[32] R. R. Jones, D. You, and P. H. Bucksbaum, Phys. Rev. Lett. **70**, 1236 (1993).
[33] R. R. Jones, Phys. Rev. Lett. **76**, 3927 (1996).
[34] A. Wetzels, A. Gürtler, H. G. Muller, and L. D. Noordam, Eur. Phys. J. D **14**, 157 (2001).
[35] M. B. Campbell, T. J. Bensky, and R. R. Jones, Phys. Rev. A **59**, R4117 (1999).
[36] Y. Song, F. M. Guo, S. Y. Li, J. G. Chen, S. L. Zeng, and Y. J. Yang, Phys. Rev. A **86**, 033424 (2012)
[37] G. G. Balint-Kurti, C. L. Ward, and C. C. Marston, Comput. Phys. Commun. **67**, 285 (1991).
[38] A. Wetzels, A. Gürtler, L. D. Noordam, F. Robicheaux, C. Dinu, H. G. Muller, M. J. J. Vrakking, and W. J. van der Zande, Phys. Rev. Lett. **89**, 273003 (2002).
[39] M. D. Feit, J. A. Fleck, Jr., and A. Steiger, J. Comput. Phys. **47**, 412 (1982).
[40] C. F. de Morisson Faria, M. Dörr, W. Becker, and W. Sandner, Phys. Rev. A **60**, 1377 (1999).